Effect of temperature on C-S-H gel nanostructure in white cement

I.F Sáez del Bosque[*1].; S. Martínez Ramírez[1,2].; M. Martín-Pastor[3]; M.T. Blanco-Varela[1].

[1] *Instituto de Ciencias de la Construcción Eduardo Torroja (IETcc-CSIC), c/ Serrano Galvache 4, 28033 Madrid, Spain*

[2] *Instituto de Estructura de la Materia (IEM-CSIC), c/ Serrano 123, 28006 Madrid, Spain*

[3] *Unidade de Resonancia Magnética, RIAIDT, Edif. CACTUS, Universidad de Santiago de Compostela, Campus sur, 15782 Santiago de Compostela, Spain*

Abstract

Different ages of white cement pastes hydrated at 100 % RH and 25ºC or 65 ºC were characterised with ^{29}Si MAS NMR spectroscopy. The findings showed that raising the curing temperature from 25ºC to 65 ºC accelerated hydration of the belite phase considerably, inducing a seven fold rise in its one day degree of hydration, while alite phase hydration grew by a factor of only 1.5 in the first day. Moreover, the C-S-H gel formed at the higher temperature had a longer mean chain length and a higher initial uptake of Al^{3+}. Lastly, curing at a higher temperature stabilised only one crystalline aluminate phases, calcium hemicarboaluminate.

Keywords: White Portland cement; hydration; C-S-H gel; ^{29}Si MAS NMR; temperature.

1. Introduction

Portland cement is a poly-phase material containing silicates (alite and belite), aluminate, ferrites and sulfates, whose hydration is complex and difficult to study due to the many factors

* Corresponding author. Tel.: +34 913020440; Fax: +34 913020700.

E-mail addresses: i.fuencisla@ietcc.csic.es and isa.f.saez@gmail.com (I.F. Sáez del Bosque)

involved. Some are intrinsic to the cement itself, such as its composition (differing clinker mineralogies, the use or otherwise of additions) and fineness or specific surface, while others are related to hydration conditions, including the water/cement ratio, absence or presence of admixtures and curing provisions (relative humidity and temperature). The reaction products deriving from portland cement hydration include a scantly crystalline calcium silicate hydrate known as C-S-H gel, the main binding phase in cement-based binders, as well as portlandite (CH) and smaller proportions of sulfoaluminate hydrates (AFt and AFm). Alite, is the main clinker phase, hydrates quickly and is consequently the phase that affords cement pastes their early age mechanical strength, a role it surrenders to belite in later age pastes 16).

White cement is characterised by a careful selection of the raw materials used in its manufacture, for it must ensure $L \geq 87$ whiteness, measured as specified in Spanish standard UNE (1). For that reason, white cement clinker may not contain iron in its composition, an element that acts as an effective flux in grey cement. The absence of such a flux calls for higher clinkerisation temperatures and the use of raw mixes with a lower lime saturation, i.e., to clinkers with higher proportions of belite than found in grey cement.

White cement is often used in both precast and cast-in-place architectural concrete. Applications include precast curtain walls and facing panels, terrazzo surfaces, stucco, cement paint, tile grout, and decorative concrete. It is especially suitable for exposed aggregate finishes and for making colored cements containing pigments as additions (21). Precast concrete products are manufactured at high curing temperatures. On the one hand, temperature is known to accelerate the hydration rate in all cement phases (16), raising early age strength, whereas older age performance is better in ambient- than high temperature-cured cement 16, 28). On the other, temperature modifies cement paste microstructure considerably, inducing an uneven distribution of hydration products and greater paste porosity 829, 30), while altering the composition of the pore solution (30). High temperatures likewise alter C-S-H gel composition, lowering its Ca/Si ratio (15, 16, 35); however, other authors reported that the temperature does not apparently influence in the Ca/Si (17, 25, 30).The proportions of stable cement hydration phases also change with curing temperature (13). Studies conducted by Damidot et al. (10-12) show that at ambient temperature, ettringite is the sole stable calcium sulfoaluminate, while at 50 ºC and 85 ºC, calcium monosulfoaluminate hydrate also has a stability field.

One of the techniques most commonly used to monitor portland cement hydration is isothermal conduction calorimetry (50), which records the heat released during hydration reactions and the times when they take place. Since this method does not provide information on the nanostructure of the C-S-H gel formed, however, supplementary trials such as SEM/EDS or TEM/EDS must be run to obtain information on gel composition. ^{29}Si magic angle spinning nuclear magnetic resonance (^{29}Si MAS NMR), by contrast, delivers information on C-S-H gel nanostructure and the evolution of silicate phase hydration reactions.

The present study aimed to analyse the variations in the nanostructure of the C-S-H gel obtained by hydrating white cement with a high belite content at two temperatures, and monitor the degree of hydration attained by alite and belite over time at each temperature. The laboratory technique used to this end was primarily ^{29}Si MAS NMR.

2. Experimental

The white cement used in this study, classified as BL I 52.5 R in Spanish standard UNE 80305 (2) , was provided by CEMEX. Its chemical composition is given in Table 1.

Table 1. XRF chemical analysis of white cement BL I 52.5 R

Table 2 lists the mineralogical composition of the cement calculated by substituting the percentages of the oxides identified with XRF (Table 1) in the Bogue formulas (7), modified to include the Ca^{2+} ions found not only in the silicate (alite and belite) and aluminate (tricalcium aluminate and ferrite) phases, but also in $CaCO_3$ and $CaSO_4 \cdot 2H_2O$.

Table 2. Mineralogical composition of white cement (modified Bogue analysis)

White cement was hand-mixed at a water/cement (w/c) ratio of 0.425 for 3 minutes. The pastes were cured at 100 % relative humidity (RH) at 25 ºC or 65 ºC. The hydration reaction was detained at 1, 28, 62 or 182 days with acetone, followed by vacuum drying for approximately 1.5 hours.

The hydrated pastes were studied on a BRUKER AVANCE-400 (9.4 T) ^{29}Si MAS NMR spectrometer operating at 79.4 MHz for ^{29}Si. The samples were packed into 7-mm ZrO_2 rotors (active sample volume, 150 mg). Free induction decay (FID) signals were acquired via magic angle spinning and continuous pulse proton decoupling at a field strength ($\gamma B_2/2\pi$) of 2 kHz. The other instrumental settings were: pulse length, 7 µs; spinning rate, 4 kHz; scans, 128. Kaolin (δ = -91.5 ppm), referenced to TMS (δ = 0 ppm), was used as the external control for chemical shift in all the ^{29}Si MAS NMR experiments. The relaxation delay (d_1) was 60 seconds, a value

that met the quantitativity criterion, for it was five times greater than the longitudinal relaxation (T_1) as calculated with the saturation-comb experiment (33).

Longitudinal ^{29}Si relaxation times (T_1) were measured for both the anhydrous WPC and the paste hydrated for 62 days at 25 ºC (BL62d). The saturation-comb consisted of a train of 25 $\pi/2$ saturation pulses of duration 7 µs separated by delays of 30 ms. Spectra were obtained for the anhydrous WPC and BL62d with the following values of variable delay (τ): 1, 2, 4, 6, 10, 15 20, 40, 60 and 100 s. Each spectrum in the series was acquired with 16 scans at a MAS spinning rate of 6 kHz. A relaxation delay of 60 s was applied to prevent excessive probe and sample heating. The anhydrous WPC findings were: for belite, $T_1 = 9 \pm 2$ s; T_1 was not calculated for alite, for according to the literature (43), it yields shorter T_1 values than belite. The T_1 values found in paste BL62d were 6 ± 1 s and 7 ± 1 s, respectively, for the Q^1 and Q^2 units in the C-S-H gel formed.

The solid-state ^{27}Al MAS NMR experiments were performed on a Varian Agilent INOVA 17.6 T spectrometer (^1H resonance frequency, 750 MHz; ^{27}Al resonance frequency, 195.36 MHz) fitted with a T3 MAS solid probe. The samples were loaded into 3.2 mm zirconia rotors. ^{27}Al MAS spectra were acquired using a single pulse sequence, a pulse width of 1 µs ($\gamma B1/2\pi$ = 60 kHz), spinning speeds of about 22 kHz, a 3 s relaxation delay and 512 scans. ^{27}Al MAS NMR chemical shift was zeroed to the external standard used, a 1.0 M aqueous solution of $AlCl_3 \cdot 6H_2O$.

Spectrum processing and signal deconvolution-based quantitative integration were performed with MestRe-C v3.9 (8) software.

Fourier transform infrared spectroscopy (FTIR) spectra were recorded on a NICOLET 6700 FT-IR series spectrophotometer. Specimens were prepared by mixing 1mg of sample with 300 mg of KBr. Spectral analysis was performed over the wavenumber range 4 000–400 cm^{-1} at a resolution of 4 cm^{-1}.

Powder X-ray diffraction (XRD) studies were conducted on a Bruker D8 Advance diffractometer, consisting of a high voltage, 3 kW generator, a (1.54 Å CuKα) copper anode X-ray tube normally operating at 1.54 kV and 50 mA, a Lynxeye detector with a 3 mm antiscatter slit and a (0.5 %) Ni K-beta filter. It was not fitted with a monochromator (i.e., $K\alpha_2$ was not

eliminated). Readings were taken at 2θ diffraction angles ranging from 5 to 60º, with a step size of 0.019º and a count time per step of 0.5 s.

PhreqeeC software was used to determine the concentration of aluminium of some phases in equilibrium in a closed system at 25ºC and 65ºC. The solubility product data for all the compounds at 25ºC were taken from Stronach (45) (Table 3), and the solubility product data at 65ºC were directly calculated with PhreqeeC sofware according to Van't Hoff equation.

3. Results and discussion

The ^{29}Si MAS NMR spectrum for the anhydrous cement (Figure 1) was characterised by a relatively narrow signal at around -71.3 ppm attributed to belite (9, 20) and a series of wide signals between -66 ppm and -77 ppm, attributed to alite (23). These signals were much wider than the bands characteristic of pure tricalcium and dicalcium silicate, due to the uptake of ions such as Al^{3+}, Mg^{2+} and Fe^{3} in the crystalline structure of these two phases (48) during their formation in the furnace.

The experimental spectrum was simulated with three bands: a narrow signal at -71.3 ppm, associated with belite (that can be likened to β-C_2S) and two wider signals at -69.89 ppm and -73.51 ppm, attributed to alite (which can be likened to C_3S). This deconvolution process is similar to the method proposed by Rawal et al. (37), who found an optimal simulation for alite with only two signals, using T_1- filtered ^{29}Si spectra, instead of the nine bands with variable Lorentzian/Gaussian ratios used by other authors in their simulations (36, 43). Establishing appropriate deconvolution parameters for the anhydrous WPC spectrum is instrumental to obtaining meaningful or logical results, for while good fits can be obtained using wholly incongruent parameters, the molar percentages obtained for the alite and belite phases will vary widely.

The molar percentages obtained for alite and belite after deconvolution of the ^{29}Si MAS NMR spectrum for anhydrous white cement were 65.61 % and 34.39 %, respectively. Using these percentages and the total amount of SiO_2 determined with XRF, the percentages by weight for alite and belite were, respectively, 54.13 % and 21.40 %, for a belite/alite ratio of 0.395. That value concurred with the 0.393 calculated with the modified Bogue formulas (Table 2). The close correlation between the values obtained with the two techniques provided evidence of accurate deconvolution of the ^{29}Si MAS NMR spectrum for anhydrous WPC.

Figure 1. Deconvolution of the ^{29}Si MAS NMR spectrum for anhydrous WPC

C-S-H, a gel formed during WPC hydration, is characterised by a sandwiched structure, with a central layer of Ca-O flanked on both sides by finite chains of SiO_4 tetrahedra in dreierkette arrangement: sets of three, in which the two end tetrahedra share their oxygen atoms with the central Ca-O core, while the central or bridging tetrahedron joins the other two (39, 46, 47). Although C-S-H gel consists essentially of Si^{4+}, O^{2-} and Ca^{2+} ions, it may also contain different ions present in the starting materials, such as Al^{3+}, Na^{+} or SO_4^{2-} (39, 41).

Figure 2 shows the ^{29}Si MAS NMR spectra for pastes of different ages obtained by hydrating WPC at 25 ºC or 65 ºC. In NMR nomenclature, silicon tetrahedra are symbolised as Q with a superscript, n, indicating silicate connectivity, i.e., the number of oxygen atoms shared with the adjacent silicon atoms (27). Further to that system, these spectra contained: Q^0, isolated tetrahedra (bands at -67 ppm to -76 ppm associated with anhydrous alite and belite); Q^1, chain-end tetrahedra or dimers (signal at -79 ppm); and Q^2, mid-chain groups where both adjacent tetrahedra are occupied by silicon atoms (at -85 ppm), The latter two, attributed to the C-S-H gel formed during cement hydration (6, 38), overlapped with a third signal at around -82 ppm, associated with Q^2(1Al) units, i.e, mid-chain groups in which one of the adjacent tetrahedra contained aluminium. This final signal was not clearly distinguishable on these spectra but was necessary to accurately simulate the experimental ^{29}Si MAS NMR spectrum with deconvolution techniques. The presence of this tetrahedrally coordinated Al^{3+} in lieu of the Si^{4+} in the bridge position, -Al(IV)-, was corroborated by the analysis of the ^{27}Al MAS NMR spectra reproduced in Figure 3. Note the signal at around 70 ppm, associated with Al^{3+}, in addition to the signals characteristic of hydrated aluminates in the 0 to 20 ppm range, denoting octahedrally coordinated Al^{3+}, -Al(VI)- (5, 44). A signal observed at around 35 ppm was attributed to pentacoordinated Al^{3+} -Al(V)- , resulting from the replacement of Ca^{2+} ions in the interlayered C-S-H structure (18). Other authors (40), using transmission electron microscopy and energy dispersive spectroscopy (TEM/EDS), have identified the presence of aluminium in the composition of C-S-H gel.

Figure 2. ^{29}Si MAS NMR spectra for WPC paste cured at (a) 25 ºC and (b) 65 ºC

Figure 3. ^{27}Al MAS NMR spectrum for 62 day WPC paste cured at 25 ºC.

177 The percentages of the Q^n units present in the various types of paste, determined by
178 deconvoluting the spectra, are given in Table 4. Two deconvolution procedures were used,
179 applying other authors' proposals. On the one hand, a previously described method similar to
180 the system proposed by Rawal et al. (37) was used to simulate the signals for the anhydrous
181 cement remaining in the paste. On the other, a procedure based on a proposal by Andersen et
182 al. (4) was deployed to simulate the C-S-H gel signal. This latter method consists essentially of
183 setting initial values for the peak associated with the Q^2(1Al) units in the C-S-H gel in all the
184 hydration series to simulate the experimental spectrum. In other words, the following
185 parameters were maintained constant: a) the Lorentzian/Gaussian ratio (at 0.5); b) signal
186 position (chemical shift); and c) peak width (in a given Hz range). To process these spectra, the
187 Q^2(1Al) peak width was maintained in the 220 ± 25 Hz range. This value was the mean found
188 for five deconvolutions each of the spectra for a given hydration time and curing temperature
189 and very similar to the value calculated by Andersen et al. (4). Particular care was taken in
190 deconvoluting the peak associated with belite, the width of whose signal was held constant
191 across the entire hydration series at the value obtained in the spectrum for anhydrous cement.
192 Some authors (4, 37) use an extra signal at around -73.2 ppm throughout WPC hydration to
193 simulate the remaining unreacted silicate phases, which they associate with γ-C_2S. No such
194 signal was used to deconvolute the spectra analysed in this study because the bands
195 characteristic of that phase (49) were not detected with FTIR (Figure 4). These bands appear at
196 950 cm^{-1} (asymmetric stretching band generated by the Si-O bonds in the SiO_4, ν_3) and at 564
197 cm^{-1} and 492 cm^{-1} (bending bands generated by the ν_4 in SiO_4), and do not overlap with other
198 silicate phase signals (alite and β-C_2S). No diffraction line whatsoever was observed for γ-C_2S in
199 the XRD studies, either.

200 **Figure 4. FTIR spectrum for anhydrous WPC and the γ-C_2S polymorph.**

201 As hydration advanced, the Q^0 unit signals associated with the anhydrous silicate
202 phases declined as a whole, while the formation of Q^1 and Q^2 units intensified at both curing
203 temperatures (Figure 5 and Table 4). The temperature induced intensification of Q^2 unit
204 formation and decline in Q^1 unit formation in the 28 day materials was significant, for it inferred
205 changes in C-S-H gel nanostructure with temperature. The Q^2(1Al) units, in turn, were observed
206 to form more actively with temperature at early ages only, an indication that temperature

favoured the initial uptake of Al^{3+} in the C-S-H gel, which remained essentially flat after approximately 62 days. It was probably due to faster reaction of C_3A with rise cured temperature according to previous studies (16).

Table 4. ^{29}Si MAS NMR for WPC pastes at 25 ºC and 65 ºC

Figure 5. Variation in the proportion of Q^n units in the C-S-H gel formed during WPC hydration at 25 ºC and 65 ºC.

In the literature, the degree of cement hydration (β) or the amount of C-S-H gel formed is generally found from the following equation: $\beta = Q^1+Q^2 = 100-Q^0$ (3, 26). This equation showed that, at all ages, total silicate hydration in the paste rose with temperature (Figure 6 and Table 4), with hydration values of close to 100 % in the 182 day specimens hydrated at 65 ºC. Nonetheless, the information provided by this equation is not broken down into the alite and belite phases. The degree of hydration in these phases was consequently calculated with the equation proposed by Justnes et al (24), in which the relative areas of the signals obtained by deconvoluting the ^{29}Si MAS NMR spectra for the cement pastes -A(t)- are divided to the relative area of the same signals in the spectrum for the anhydrous cement -A(t=0)-, according to the following equation: hydration degree of Alite/belite (%) = [1 – (A(t)/A(t=0))] x 100.

Figure 7 shows the variation in the degree of silicate hydration over time in BL I 52.5 R cement, at both temperatures. As expected, the degree of alite and belite hydration rose with curing time and temperature. Hydration was consistently higher in alite than in belite at any given temperature and curing age due to the difference in their reaction kinetics. Emphasize that the temperature affected the belite hydration rate intensely, especially at the initial ages. At day 1 belite hydration grew seven-fold when the curing temperature was raised, while alite only rose by a factor of 1.5. Finally, the degree of belite hydration in pastes cured at 25 ºC was higher than reported in the literature (37).

Figure 6. Variation in total cement paste hydration with curing time at 25 ºC and 65 ºC.

Figure 7. Degree of hydration in (a) alite and (b) belite in WPC pastes cured at 25 ºC and 65 ºC.

Moreover, the relationship between the degree of total hydration and the percentage of both Q^1 and Q^2 units in the C-S-H gel (Figure 8) proved to be linear, with correlation coefficients (R^2) ranging from 0.935 to 0.996. The slope of the line for the Q^1 units declined with rising curing

237 temperature, whereas the slope for the Q^2 units rose significantly, an indication that temperature
238 affected not only reaction kinetics but also the structure of the gel formed.

239 **Figure 8. Q^1 and Q^2 units in the C-S-H gel formed during WPC hydration vs total degree of**
240 **silicate hydration at 25 ºC and 65 ºC.**

241 Another important characteristic of C-S-H gels is their mean chain length (MCL). Figure
242 9 shows that as hydration progressed, the C-S-H gels formed had longer MCLs, suggesting that
243 the polymerisation took place in keeping with the usual pattern: two monomers joining to form a
244 dimer; monomer + dimer + dimer joining to form a pentamer and, less frequently, monomer +
245 dimer + pentamer joining to form an octamer (22). MCL rose significantly with curing
246 temperature, with 182 day gels cured at 65 ºC exhibiting mean chain lengths of 6.13 compared
247 to 4.27 in the pastes cured at 25 ºC. In other words, at 65 ºC the gels formed consisted primarily
248 of pentameric silicates and a smaller proportion of octamers, whereas at 25 ºC they comprised
249 essentially dimers and pentamers. The increase in MCL with curing temperature has been
250 reported in C_3S (42) and WPC (32) hydration studies, although the latter authors made no
251 mention of any steep rise in the degree of belite hydration with curing temperature.

252 The chain lengths found here for the pastes cured at 25 ºC were similar to the findings
253 observed by other authors (32). They were somewhat higher, however, than reported by
254 Andersen et al. (4), for white cement hydrated at 20 ºC, even though these authors used the
255 same deconvolution procedure and chemical shift and peak width (in Hz) values as in this study,
256 as well as a constant L/G ratio of 0.5 to simulate the Q^2(1Al) signal.

257 **Figure 9. Variation in MCL for the C-S-H gels obtained by hydrating WPC at different**
258 **curing temperatures.**

259 Some authors have noted that longer chain lengths could be obtained by increasing the
260 amount of tetrahedrally coordinated Al^{3+} taken up in the C-S-H gel, because Al^{3+} is located in
261 the bridging tetrahedra. The Al(IV)/Si ratio (Figure 10) found with the equation proposed by
262 Richardson (38) rose up to the age of 62 days in the samples cured at 25 ºC, while in the
263 samples hydrated at 65 ºC, the Al(IV)/Si ratio was much higher at early ages and declined with
264 hydration time. Temperature changes the proportions of stable aluminate phases and enhances
265 the solubility of several aluminate hydrates, which would explain these results.

Further to the XRD findings, the 1 day pastes hydrated at both curing temperatures contained calcium hemicarboaluminate (Hc) as the sole crystalline aluminate phase, while at 25 ºC, traces of ettringite may have been present. Over time, ettringite (AFt), co-existing with calcium monosulfoaluminate (AFm) or calcium hemicarboaluminate, crystallised in the samples cured at 25 ºC, whereas in the pastes cured at 65 ºC, only calcium hemicarboaluminate was found.

Table 5 gives the theoretical aluminium dissolved concentration for different phases in saturated aqueous solutions at the two experimental temperatures, as calculated with PhreqeeC software (34). Note that the aluminium dissolved concentration rose with temperature, according to Lothenbach (31).

Table 5. Dissolved aluminium concentration in solutions in contact with hydrated phases in cement cured at 25 ºC and 65 ºC

The aluminate phases may be assumed to react faster at 65 ºC, which would translate into a higher aluminium dissolved concentration in the water at early ages, when the rate of C-S-H gel precipitation is high. That would explain the higher initial uptake of Al^{3+} in the gel structure. Over time, the amount of aluminium dissolved available in the solution would decline, although hydration continues. The new gels formed would have a lower Al^{3+} content and consequently a lower mean Al(IV)/Si ratio.

No AFt formed at 65 ºC, nor was monosulphate obtained, while Hc was the sole crystalline aluminous phase present at all the ages studied. Hence, higher temperature led to greater sulfate ion uptake/absorption in the C-S-H gel (14, 19). Lastly, either monosulphate or hemicarboaluminate was observed (Figure 11).

Figure 10. Variation in the Al(IV)/Si ratio in the C-S-H gel formed during WPC hydration at 25ºC and 65ºC.

Figure 11. Diffractograms for the pastes obtained by hydrating WPC at 25 ºC and 65 ºC, where CH is portlandite, AFt is ettringite, AFm is calcium sulfoaluminate and Hc is calcium hemicarboluminate.

4. Conclusions

The present study used ^{29}Si nuclear magnetic resonance to determine the effect of temperature (25 ºC and 65 ºC) on alite and belite hydration, the nanostructure of the C-S-H gel and the phase ratios obtained in a white cement.

- Temperature accelerated the hydration rate of both silicates, but belite much more intensely, for its degree of hydration was up to seven times greater in the 1 day samples cured at 65 ºC than in the same age samples cured at 25 ºC.
- The C-S-H gels obtained at 65 ºC had a much longer mean chain length than the gels obtained at 25 ºC due to the steep rise in Q^2 unit, and a decline in Q^1 unit, formation in the former.
- The proportion of Al^{3+} taken up in the C-S-H gels obtained at 65 ºC was initially very high and declined with hydration time, while in the gels obtained at 25 ºC uptake was initially lower and grew with curing time.
- The pastes hydrated at 25 ºC contained ettringite together with calcium monosulfoaluminate hydrate or calcium hemicarboaluminate hydrate, while the latter was the sole crystalline aluminate present in the pastes cured at 65 ºC.

◆ Acknowledgements

This research was funded by the Spanish Ministry of Education and Science (MAT2006-11705, CONSOLIDER: CSD2007-00058 and PIE: 201160E103) and the Regional Government of Madrid (Geomaterials Programme, S2009/MAT-1629). Research fellowship BES-2007-16686 is gratefully acknowledged. The authors also wish to thank Dr. Isabel Sobrados for conducting the ^{29}Si MAS NMR spectra and Dr. Paula M. Carmona-Quiroga for her assistance with the thermodynamic calculations.

◆ References

1.- AENOR (2011). Cement - Part 1: Composition, specifications and conformity criteria for common cements. 1-40.

2.- AENOR (2012). Methods of testing cements. Physical analysis. Colour determination in clinkers and white cements. 1-8.

3.- Al-Dulaijan SU, Parry-Jones G, Al-Tayyib A-HJ, Al-Mana AI (1990). ^{29}Si Magic-Angle-Spinning Nuclear Magnetic Resonance Study of Hydrated Cement Paste and Mortar. J. Am. Ceram. Soc. 73: 736-739.

4.- Andersen MD, Jakobsen HJ, Skibsted J (2004). Characterization of white Portland cement hydration and the C-S-H structure in the presence of sodium aluminate by ^{27}Al and ^{29}Si MAS NMR spectroscopy. Cem. Concr. Res. 34: 857-868.

5.-Andersen MD, Jakobsen HJ, Skibsted J (2006). A new aluminium-hydrate species in hydrated Portland cement characterized by ^{27}Al y ^{29}Si MAS NMR spectroscopy. Cem. Concr. Res. 36: 3-17.

6.- Barnes J R, Clague, DH Clayden NJ, Dobson CM, Hayes CJ, Groves GW, Rodger SA. (1985). Hydration of Portland cement followed by 29Si solid-state NMR spectroscopy. J. Mate. Sci. Letters 4: 1293-1295.

7.- Bogue R H (1929). Calculation of the compound in portland cement. Industrial and Engineering Chmestry (Anal.) 1(2): 192-197.

8.- Cobas J C, Sardina FJ (2003). Nuclear magnetic resonance data processing: MestRe-C, a software package for desktop computers. Concepts in Magnetic Resonance A 19: 80-96.

9.- Cong X, Kirkpatrick RJ (1993). ^{17}O and ^{29}Si MAS NMR study of β-C_2S hydration and the structure of calcium-silicate hydrates. Cem. Concr. Res. 23: 1065-1077.

10.- Damidot D, Glasser FP (1992). Thermodynamic investigation of the CaO–Al2O3–CaSO4–H2O system at 50 and 85ºC. Cem. Concr. Res. 23: 1179-1191.

11.- Damidot D, Glasser FP (1995). Thermodynamic investigation of thhe CaO-Al2O3-CaSO4-CaCO3-H2O. Advances in Cement Research 27: 129-134.Antoni, M R, Rossen J, Martirena, F, Scrivener, K. (2012). Cement substituttion by a combination of metakaolin and limestone. Cem. Concr. Res. 42: 1579-1589.

12.- Damidot D, Glasser FP (1993).Thermodynamic investigation of the CaO–Al2O3–CaSO4–H2O system at 25 °C and the influence of Na2O. Cem. Concr. Res. 23: 221-238.

13.- Damidot D, Lothenbach B, Glasser FP (2011). Thermodinamics and cement science. Cem. Concr. Res. 41: 679-695.Çakr Ö, Aköz F. (2008). Effect of curing conditions on the mortars with and without GGBFS. Constr. Build. Mater. 22: 308-314.

14.- Divet L, Randriambololona R (1998). Delayed ettringite formation: the effect of temperature and basicity on the interaction of sulphate and C-S-H phase. Cem. Concr. Res. 28: 357-363.

15.- Escalante-García IJ, Sharp JH (1999). Variation in the Composition of C-S-H gel in Portland Cement pastes cured at various temperatures. J. Am. Ceram. Soc. 82: 3237-3241.

16.- Escalante-García IJ, Sharp JH (1998). Effect of temperature on the hydration of the main clinker phases in Portland cements: Part I, neat cements. Cem. Concr. Res. 28: 1245-1257.

17.- Famy, C., Scrivener K.L., Atkinsonb, A., Brough, A.R (2002). "Effects of an early or a late heat treatment on the microstructure and composition of inner C-S-H products of Portland cement mortars." Cement and Concrete Research 32: 269-278.

18.- Faucon P, Delagrave A, Petit JC, Riche, C, Marchand JM, Zanni H (1999). Aluminium incorporation in calcium silicate hydrates (C-S-H) depending on their Ca/Si ratio. J. Phys. Chem. B 103: 7796-7802.

19.- Fu Y, Xie P, Gu P, Beaudoin JJ (1994). Effect of temperature on sulphate adsorption/desorption by tricalcium silicate hydrates. Cem. Concr. Res. 22: 1428-1432.

20.- Grimer AR, Von Lampe F, Mägi M, Lippman E (1985). High-reoslution solid-state ^{29}Si NMR of polymorphs of Ca_2SiO_4. Cem. Concr. Res. 15: 467-473.

21.- Hamad BS (1995). Investigations of Chemical and Physical Poperties of White Cement Concrete. Advanced Cement Based Materials 2: 161-167.

22.- Hirljac J, Wu Z.-Q, Young JF (1983). Silicate polymerization during the hydration of alite. Cem. Concr. Res. 13: 877-886.

23.- Hjorth J, Skibsted J, Jakobsen HJ (1988). ^{29}Si MAS NMR studies of Portland cement components and effects of microsilica on the hydration reaction. Cem. Concr. Res. 18: 789-798.

24.- Justnes H, Meland I, Bjoergum JO, Krane J (1990) A 29Si MAS NMR study of the pozzolanic activity of condensed silica fume and the hydration of di- and tricalcium silicate. Adv Cem Res 3:111–116.

25.- Kjellsen KO (1996) Heat curing and post-heat curing regimes of high-performance concrete: influence on microstructure and C–S–H composition. Cem Concr Res 561 26:295–307.

26.- Le Saoût G, Lécolier E, Rivereau A, Zanni H (2006). "hemical structure of cement aged ar normal and elevated temperatures and pressures, Part I: Class G oilwell cement. Cem. Concr. Res. 36: 71-78.

27.- Lippmaa E, Mägi M, Samoson A, Engelhardt G, Grimmer, AR (1980). Structural Studies of Silicates by Solid-State High-Resolution ^{29}Si NMR. J. Am. Chem. Soc. 102: 4889-4893.

28.- López de la Fuente, JI, Palomo Sánchez A. (2004). Comportamiento mecánico-resistente del hormigón preparado en períodos estivales. Cemento y Hormigón 867: 4-13.

29.- Lothenbach B, Wieland E (2006). A thermodynamic approach to the hydration of sulphate-resisting Portland cement. Waste Manage 26(7): 706-719.

30.- Lothenbach B, Winnefeld F, Alder C, Wieland E, Lunk P (2007). Effect of temperature on the pore solution, microstructure and hydration products of Portland cement pastes. Cem. Concr. Res. 37(4): 483–491.

31.- Lothenbach B, Matschei T, Mo¨schner G, Glasser FP (2008). Thermodynamic modelling of the effect of temperature on the hydration and porosity of Portland cement. Cem Concr Res 38:1–18

32.- Martínez-Ramírez S, Frías M. (2009). The effect of curing temperature on white cement hydration. Constr. Build. Mater. 23: 1344-1348.

33.- Mundy JN, Rothman SJ (1983). Methods of Experimental Physics, Vol. 21: Solid State Nuclear Methods, Chap. 6. Orlando-Florida (USA).

34.- Parkhurst DL, Appelo CAJ. *A Computer Program for Speciation, Batch-Reaction, One-Dimensional Transport, and Inverse Geochemical Calculations.* http://wwwbrr.cr.usgs.gov/projects/GWC_coupled/phreeqc/index.html.Paul M, Glasser, FP (2000).Impact of prolonged warm (85ºC) moist cure on Portland cement paste. Cem. Concr. Res. 30: 1869-1877.

395 35.- Paul M, Glasser FP (2000) Impact of prolonged warm (85 C)moist cure on Portland cement paste.
396 CemConcr Res 30:1869–1877.

397 36.- Poulsen SL, Kocaba V, Le Saoût G, Jakobsen HJ, Scrivener K, Skibsted J (2009). Improved
398 quantification of alite and belite in anhydrous Portland cements by ^{29}Si MAS NMR: Effects of
399 paramagnetic ions. Solid State Nucl. Magn. Reson. 36: 32-44.

400 37.- Rawal A, Smith BJ, Athens L, Edwards CL, Roberts L, Gupta V, Chmelka BF (2010). Molecuar
401 Silicate and Aluminate species in anhydrous and hydrated cements. J. Am. Chem. Soc. 132: 7321-7337.

402 38.- Richardson IG (1999). The nature of C-S-H in hardened cements. Cem. Concr. Res. 29: 1131-1147.

403 39.- Richardson I.G (2004). Tobermorite/jennite- and tobermorite/calcium hydroxide-based models for the
404 structure of C-S-H: applicability to hardened pastes of tricalcium silicate, β-dicalcium silicate, Portland
405 cement, and blends of Portland cement with blast-furnance slag, metakaolin, or silica fume. Cem. Concr.
406 Res. 34: 1733-1777.

407 40.- Richardson IG, Groves GW (1992). Microstructure and microanalysis of hardened cement pastes
408 involving ground granulated blast-furnace slag. J. Mater. Sci. 27: 6204-6212.

409 41.- Richardson IG, Groves GW (1993). The incorporation of minor and trace elements into calcium silicate
410 hydrate (C-S-H) gel in hardened cement pastes. Cem. Concr. Res. 23: 131-138.

411 42.- Sáez del Bosque IF, Martín-Pastor M, Martínez-Ramírez S, Blanco-Varela MT (2013) Effect of
412 temperature on C_3S and C_3S + nanosilica hydration and C-S-H gel structure. J. Am. Ceram. Soc. 96: 957-
413 965

414 43.- Skibsted J, Jakobsen HJ (1995). Quantification of Calcium Silicate Phases in Portland Cements by
415 ^{29}Si MAS NMR Spectroscopy. J J Chem. Soc., Faraday Trans. 91(24): 4423-4430.

416 44.- Skibsted J, Henderson E, Jakobsen HJ (1993). Characterization of calcium aluminate phases in
417 cements by aluminum-27 MAS NMR spectroscopy.Inorganic Chemistry 32: 1013-1027.

418 45.- Stronach SA (1996). Thermodynamic modelling and phase relations of cementitious systems. Thesis
419 (PhD). University of Aberdeen.

420 46.- Taylor, H. F. W. (1986). Proposed structure for calcium silicate hydrate gel. J. Am. Ceram. Soc. 69:
421 464-467.

422 47.- Taylor HFW (1993). Nanoestructure of C-S-H: Current status. Adv. Cem. Based Mater. 1: 38-46.

423 48.- Taylor HF W (1997). Cement Chemistry. London, U.K.

424 49.- Vázquez Moreno T (1980). Aplicaciones prácticas de la espectroscopía de absorción infrarroja en el
425 estudio de los crudos, del clinker y del cemento portland anhidro. Mater. Construcc. 179: 101-110.

426 50.- Zákoutský J, Tydlitát V, Cerný R. (2012). Effect of temperature on the early-stage hydration
427 characteristics of Portland cement: A large-volume calorimetric study. Constr. Build. Mater. 36.

428

FIGURE CAPTIONS

Figure 1. Deconvolution of the ^{29}Si MAS NMR spectrum for anhydrous WPC

Figure 2. ^{29}Si MAS NMR spectra for WPC paste cured at (a) 25 ºC and (b) 65 ºC

Figure 3. ^{27}Al MAS NMR spectrum for 62 day WPC paste cured at 25 ºC.

Figure 4. FTIR spectrum for anhydrous WPC and the γ-C_2S polymorph.

Figure 5. Variation in the proportion of Q^n units in the C-S-H gel formed during WPC hydration at 25 ºC and 65 ºC.

Figure 6. Variation in total cement paste hydration with curing time at 25 ºC and 65 ºC.

Figure 7. Degree of hydration in (a) alite and (b) belite in WPC pastes cured at 25 ºC and 65 ºC.

Figure 8. Q^1 and Q^2 units in the C-S-H gel formed during WPC hydration vs total degree of silicate hydration at 25 ºC and 65 ºC.

Figure 9. Variation in MCL for the C-S-H gels obtained by hydrating WPC at different curing temperatures.

Figure 10. Variation in the Al(IV)/Si ratio in the C-S-H gel formed during WPC hydration at 25ºC and 65ºC.

Figure 11. Diffractograms for the pastes obtained by hydrating WPC at 25 ºC and 65 ºC, where CH is portlandite, AFt is ettringite, AFm is calcium sulfoaluminate and Hc is calcium hemicarboluminate.

Table 1. XRF chemical analysis of white cement BL I 52.5 R

SiO_2	Al_2O_3	Fe_2O_3	MgO	CaO	Na_2O	SO_3	K_2O	TiO_2	P_2O_5	LOI
21.71	4.85	0.32	0.88	65.08	0.15	3.82	0.57	0.12	0.06	2.387

LOI: loss on ignition at 1 000 ºC

Table 2. Mineralogical composition of white cement (modified Bogue analysis)

Phase	WPC (wt%)
C_3S	54.32
C_2S	21.37
C_3A	12.31
C_4AF	0.98

Table 3: Solid phase chemical equilibrium constants at 25ºC

Mineral	Dissolution reaction	Log K
Portlandite	$Ca(OH)_2 + 2\ H^+ = Ca^{2+} + 2\ H_2O$	22.82
C_3AH_6	$Ca_3Al_2O_6{:}6H_2O + 12\ H^+ = 3Ca^{2+} + 2\ Al^{3+} + 12\ H_2O$	78.66
Ettringite	$Ca_6Al_2S_3O_{24}H_{12}{:}26H_2O + 12\ H^+ = 6\ Ca^{2+} + 2\ Al^{3+} + 3\ SO4^{2-} + 38\ H_2O$	55.22
Hemicarboaluminate	$Ca_4Al_2CO_9{:}11H_2O + 12\ H^+ = 4\ Ca^{2+} + 2\ Al^{3+} + CO3^{2-} + 17\ H_2O$	69.86

Table 4. ^{29}Si MAS NMR for WPC pastes at 25 ºC and 65 ºC

Temperature (ºC)	Time (days)	Q^n (%)				MCL	β (%)	Al_{IV}/Si
		Q^0	Q^1	Q^2	$Q^2(1Al)$			
25	1	62.24	22.75	10.73	4.28	3.51	37.76	0.057
	28	28.07	40.33	18.64	12.95	3.89	71.93	0.090
	62	23.56	39.82	21.87	14.75	4.20	76.44	0.096
	182	19.26	41.53	23.17	16.04	4.27	80.74	0.100
	Time (days)	Q^n (%)				MCL	β (%)	Al_{IV}/Si
		Q^0	Q^1	Q^2	$Q^2(1Al)$			
65	1	31.36	32.04	20.23	16.37	4.76	68.64	0.119
	28	14.00	33.13	33.74	19.13	5.77	86.00	0.111
	62	7.51	34.64	42.20	15.65	5.79	92.49	0.085
	182	~0*	35.22	48.87	15.91	6.13	100	0.080

* Very low intensity signal, close to noise level, therefore regarded as approximately zero

Table 5. Dissolved aluminium concentration in solutions in contact with hydrated phases in cement cured at 25 ºC and 65 ºC

	Al concentration (mmol/kg solvent)		pH	
Dissolved phase	**25 ºC**	**65 ºC**	**25 ºC**	**65 ºC**
AFt	$5.536{\cdot}10^{-4}$	$5.177{\cdot}10^{-3}$	11.002	10.845
Hc	$2.453{\cdot}10^{-3}$ ↓	$5.466{\cdot}10^{-2}$ ↓	11.719	11.898
C_3AH_6	$2.477{\cdot}10^{-3}$ ↓	$7.635{\cdot}10^{-2}$	11.632	11.943
AFt + Hc + CH	$1.964{\cdot}10^{-5}$ ↓	$1.163{\cdot}10^{-2}$ ↓	12.472	12.167
AFt + CH	$6.675{\cdot}10^{-6}$	$1.392{\cdot}10^{-4}$	12.472	12.173
Hc + CH	$1.894{\cdot}10^{-5}$ ↓	$1.163{\cdot}10^{-2}$ ↓	12.472	12.167
AFt + Hc	$2.453{\cdot}10^{-3}$ ↓	$5.466{\cdot}10^{-2}$ ↓	11.719	11.898

↓ **Other phases precipitated**

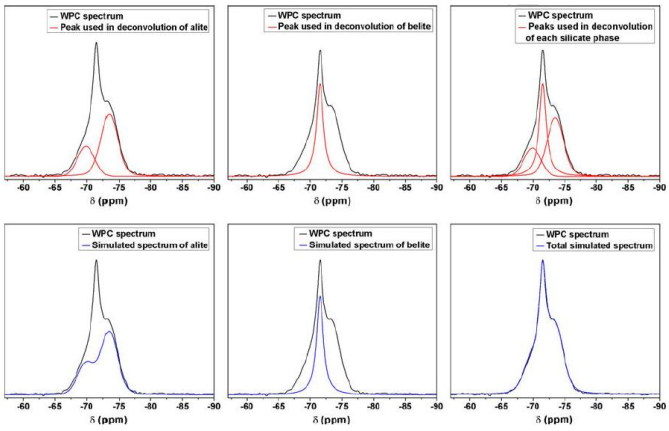

Figure 1

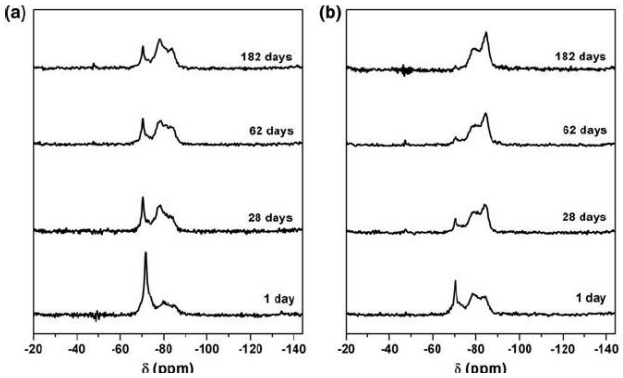

Figure 2

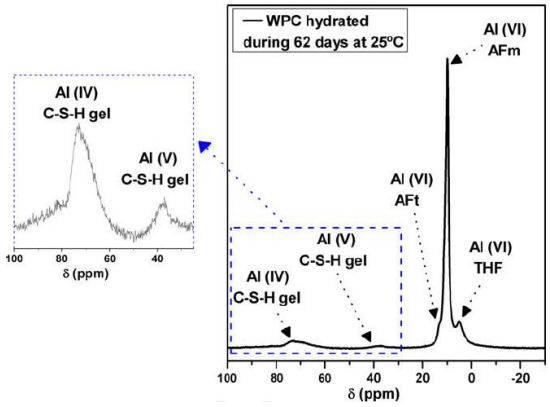

Figure 3

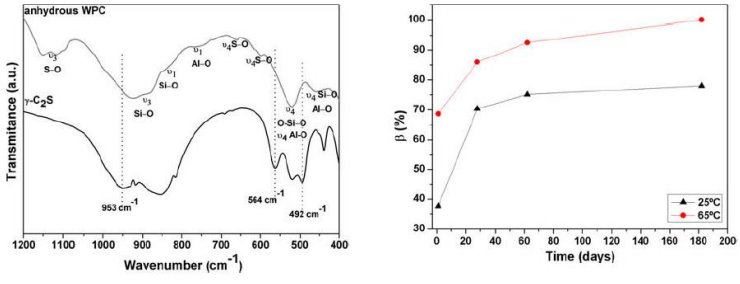

Figure 4

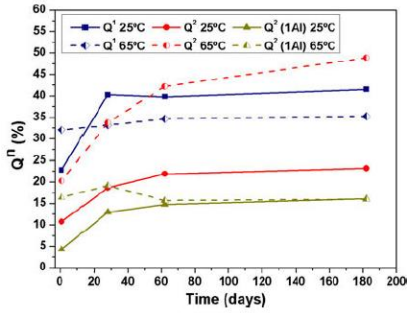

Figure 5

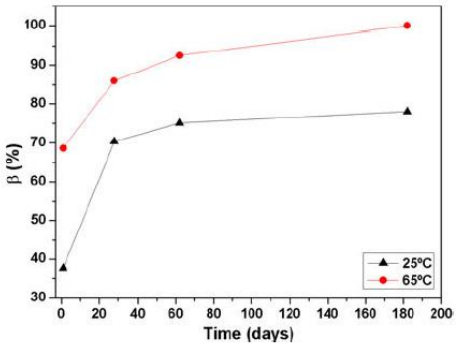

Figure 6

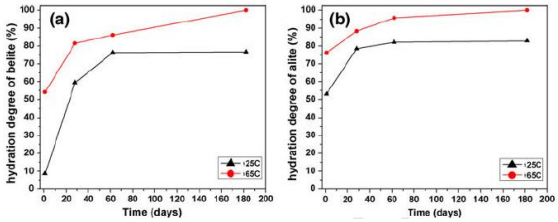

Figure 7

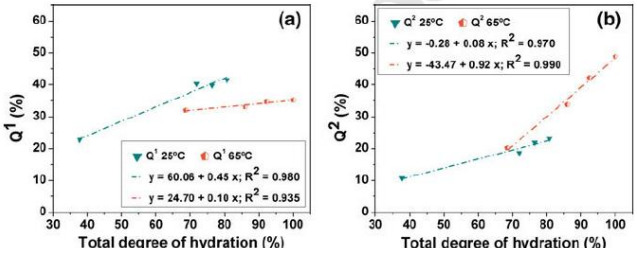

Figure 8

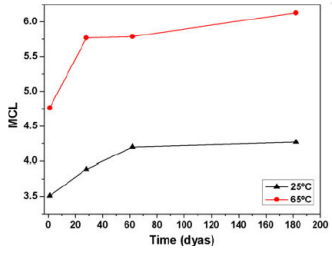

Figure 9

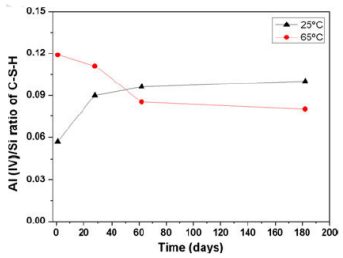

495

496 Figure 10

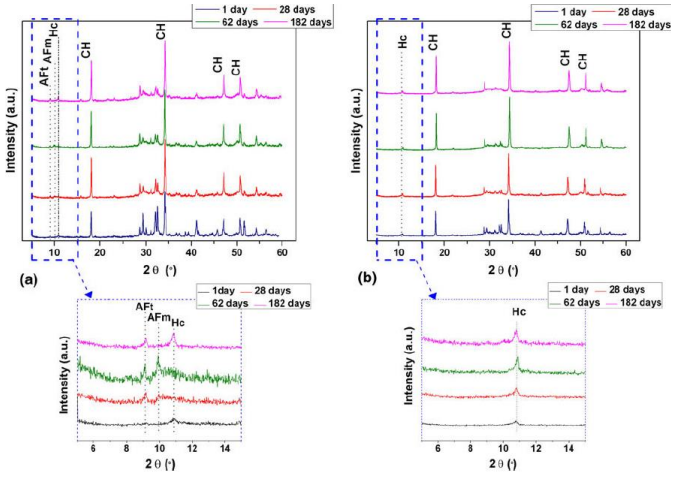

497

498 Figure 11

499